are relatively more efficient and precise than the existing Kirchhoff-type triangular elements. The nonlinear stability behaviour of shells is presently under investigation with the use of this element. The results obtained so far are excellent.

References

[1] Gallagher, R. H., "Analysis of Plate and Shell Structures," *Proceedings of the ASCE Symposium*, Civil Engineering, Vanderbilt University, Nashville, Tenn., 1969, pp. 155–205.

[2] Oden, J. T. and Wempner, G. A., "Numerical Analysis of Arbitrary Shell Structures under Arbitrary Static Loading," Tech. Rept. 47, Nov. 1967, University of Alabama Research Institute, Huntsville, Ala.

[3] Dhatt, G., "Numerical Analysis of Thin Shells by Curved Triangular Elements Based on Discrete Kirchhoff Hypothesis," *Proceedings of the ASCE Symposium*, Civil Engineering, Vanderbilt University, Nashville, Tenn., 1969, pp. 255–278.

[4] Bonnes, G. et al., "Curved Triangular Elements for the Analysis of Shells," *Proceedings of the Second Conference on Matrix Methods in Structural Mechanics*, AFFDL-TR-68-150, Air Force Flight Dynamics Lab., Wright-Patterson AFB, Ohio, 1968, pp. 617–640.

[5] Stricklin, J. A. et al., "A Rapidly Converging Triangular Plate Element," *AIAA Journal*, Vol. 7, No. 1, Jan. 1969, pp. 180–181.

[6] Dhatt, G., "Numerical Analysis of Thin Shells of Arbitrary Shape," *Proceedings of the Second Canadian Conference on Applied Mechanics*, University of Waterloo, Waterloo, Canada, 1969, pp. 95–96.

[7] Bonnes, G., "Analyse des Voiles Minces par Elements Finis Courbés," D.Sc. dissertation, July 1969, Département de Génie Civil, Université Laval, Québec, Canada.

[8] Chetty, S. and Tottenham, H., "An Investigation into the Bending Analysis of Hyperbolic Paraboloid Shells," *Indian Concrete Journal*, Vol. 38, No. 7, July 1964, pp. 248–258.

Buckling of Orthotropic Annular Plates

Ernest B. Uthgenannt* and Ronald S. Brand†
University of Connecticut, Storrs, Conn.

Introduction

THE buckling of orthotropic circular plates, due to in-plane compressive loads, has been investigated by Woinowski-Krieger,[1] Mossakowski,[2] and Pandalai and Patel.[3] Extending the analysis to include annular plates requires additional boundary conditions at the inner edge and thereby increases the mathematical complexity of the governing equation. In each of the cited papers, the critical buckling loads were determined from characteristic equations obtained from series solutions of the governing deflection equation. Including the inner-boundary conditions prohibits a series solution. Therefore, this Note employs finite-difference equations and the Vianello-Stodola iterative procedure to solve the title problem for several boundary conditions.

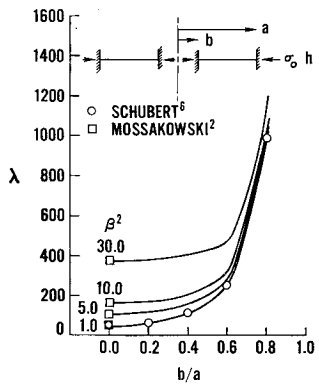

Fig. 1 Critical buckling loads, buckling parameter $\lambda = -\sigma_o h a^2/Dr$ vs b/a, both edges fixed and loaded.

Analysis

The governing axisymmetric equation in terms of the deflection w and the stresses σ_r and σ_θ is

$$\Delta w = \frac{h}{D_r}\left(\sigma_r \frac{d^2w}{dr^2} + \sigma_\theta \frac{1}{r}\frac{dw}{dr}\right) \tag{1}$$

where

$$\Delta = \frac{d^4}{dr^4} + \frac{2}{r}\frac{d^3}{dr^3} - \frac{\beta^2}{r^2}\left(\frac{d^2}{dr^2} - \frac{1}{r}\frac{d}{dr}\right)$$

r,θ = radial and circumferential coordinates, respectively; $D_r = E_r h^3/12(1 - \nu_{r\theta}\nu_{\theta r})$; $\beta^2 = E_\theta/E_r$; E_θ, E_r = moduli of elasticity in the circumferential and radial directions, respectively; $\nu_{r\theta}, \nu_{\theta r}$ = Poisson's ratios, and h = plate thickness.

The stresses can be derived independently of the deflection from the compatibility equation, the stress-strain relations, and the equilibrium equation. Thus, the equations to determine the stresses are given by

$$d^2\sigma_r/dr^2 + (3/r)(d\sigma_r/dr) + (1 - \beta)/r^2\ \sigma_r = 0 \tag{2}$$

and

$$d/dr(r\sigma_r) = \sigma$$

Integrating Eq. (2) gives

$$\sigma_r = C_1 r^{(\beta-1)} + C_2 r^{-(\beta+1)}$$

where C_1 and C_2 are determined from the loading conditions at the inner edge ($r = b$) and the outer edge ($r = a$). Substituting the stresses into Eq. (1) and writing the resulting equation in nondimensional form[4] gives

$$\nabla w + \lambda\left[(C_3\rho^{\beta-1} + C_4\rho^{-\beta-1})\frac{d^2w}{d\rho^2} + \frac{\beta}{\rho}\times (C_3\rho^{\beta-1} - C_4\rho^{-(\beta+1)})\frac{dw}{d\rho}\right] = 0 \tag{3}$$

where:

∇ = Δ with ρ substituted for r
$\lambda = -\sigma_o h a^2/D_r$
$C_3 = C_1 a^{\beta-1}/\sigma_o$
$C_4 = C_2 a^{-(\beta+1)}/\sigma_o$
$\rho = r/a$

Nontrivial solutions of Eq. (3) exist for particular values of the eigenvalue λ. The first eigenvalue determines the lowest critical buckling load σ_o.

Method of Solution

Equation (3) can be reduced to a second-order equation in terms of slope plus a constant of integration. For ease in

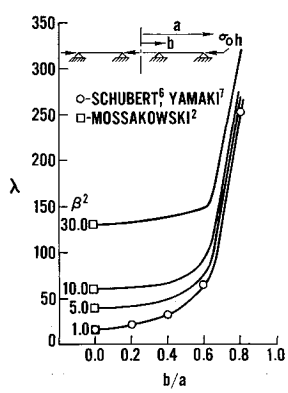

Fig. 2 Critical buckling loads, buckling parameter $\lambda = -\sigma_o h a^2/Dr$ vs b/a, both edges simply-supported and loaded.

Received June 18, 1970.

* Graduate Student; now Assistant Project Engineer, Pratt & Whitney Aircraft Division, United Aircraft Corporation, East Hartford, Conn.; also Lecturer, University of Connecticut Graduate School Extension.

† Professor and Head, Mechanical Engineering Department.

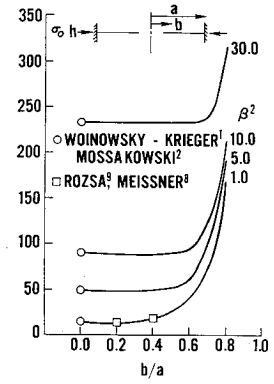

Fig. 3 Critical buckling loads, buckling parameter $\lambda = -\sigma_o h a^2/Dr$ vs b/a, outer edge fixed and loaded, inner edge free.

handling the boundary conditions it is preferred here, however, to proceed with the solution of Eq. (3). Writing Eq. (3) in finite-difference form and collecting coefficients of terms with like subscripts gives

$$w_iA_i + w_{i+1}C_i + w_{i+2}E_i + w_{i-1}F_i + w_{i-2}H_i - \lambda(w_iB_i + w_{i+1}D_i + w_{i-1}G_i) = 0,\ i = 1,n \quad (4)$$

where, for an annular plate with inner and outer edges loaded,

$$\begin{aligned}
A_i &= 6/t^4 + 2\beta^2/t^2\rho_i^2 \\
B_i &= -2(D1\rho_i^{\beta-1} + D2\rho_i^{-\beta-1}) \\
C_i &= -4/t^4 - 2/t^3\rho_i - \beta^2/t^2\rho_i^2 + \beta^2/2t\rho_i^3 \\
D_i &= [D1 + (D3/\rho_i)]\rho_i^{\beta-1} + [(D2 + (D4/\rho_i)]\rho_i^{-\beta-1} \\
E_i &= 1/t^4 + 1/t^3\rho_i \\
F_i &= -4/t^4 + 2/t^3\rho_i - \beta^2/t^2\rho_i^2 - \beta^2/2t\rho_i^3 \\
G_i &= [D1 - (D3/\rho_i)]\rho_i^{\beta-1} + [D2 - (D4/\rho_i)]\rho_i^{\beta-1} \\
H_i &= 1/t^4 - 1/t^3\rho_i
\end{aligned}$$

and

$$\begin{aligned}
i &= \text{any mesh point} \\
t &= \text{mesh size} \\
n &= \text{number of mesh points} \\
D1 &= -(1/t^2)D5 \\
D2 &= -(1/t^2)\ D6 \\
D3 &= -(1/2t)\beta\ D5 \\
D4 &= -(1/2t)\ \beta\ D6 \\
D5 &= [1 - (b/a)^{-\beta-1}]/[(b/a)^{-\beta-1} - (b/a)^{\beta-1}] \\
D6 &= [(b/a)^{\beta-1} - 1]/[(b/a)^{-\beta-1} - (b/a)^{\beta-1}]
\end{aligned}$$

Equation (4) can be written in matrix form as

$$([M] - \lambda[N])(w) = 0 \quad (5)$$

where $[M]$ = matrix whose elements are A_i, C_i, E_i, F_i, and H_i; $[N]$ = matrix whose elements are B_i, D_i and G_i; and (w) = column vector of the displacement.

The boundary conditions determine the first two and last two rows of matrix $[M]$ and the first and last rows of matrix $[N]$. Expressing Eq. (5) in a form amenable with the Vianello-Stodola method gives

$$[C](w) = \frac{1}{\lambda}[I](w)$$

where $[C] = [M]^{-1}[N]$ and $[I]$ = identity matrix.

To determine the first eigenvalue λ the Vianello-Stodola method[5] was employed, and the computations involved were performed on a digitial computer.‡ Several mesh sizes were chosen to check convergence. Using 1–40 mesh points showed that reasonable convergence occurred in the neighborhood of 15–20 mesh points using double precision.

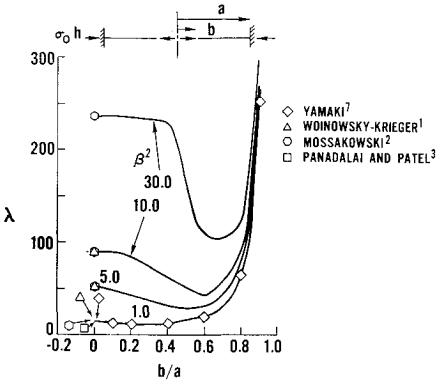

Fig. 5 Critical buckling loads, buckling parameter $\lambda = -\sigma_o h a^2/Dr$ vs b/a, outer edge fixed, inner edge free; both edges loaded.

Results

The critical buckling loads have been determined for several boundary conditions and two types of loading; they are shown in Figs. 1–6. The boundary and loading conditions are given on each figure. The parameters involved are, λ the nondimensional critical buckling load, b/a the ratio of inner to outer radius, and β^2 the ratio of moduli.

β^2 ranges from 1, the isotropic case, to 30; b/a ranges from zero, a circular plate, to 0.8, approaching a ring. In all calculations Poisson's ratios, $\nu_{r\theta} = \nu_{\theta r} = 0.3$ is used. In each figure the critical buckling loads for the isotropic cases are shown to agree with data obtained by previous investigators. Similarly, the circular plate critical buckling loads agree with previously obtained data for the range of β^2 shown. As an example, $\lambda = 14.68$ for the circular isotropic case of Fig. 3 as given by Woinowski-Krieger.[1] The value of λ from this analysis is 14.66, a difference of less than 1%.

Each figure shows the pronounced effect of the orthotropic nature of the material upon the critical buckling loads and

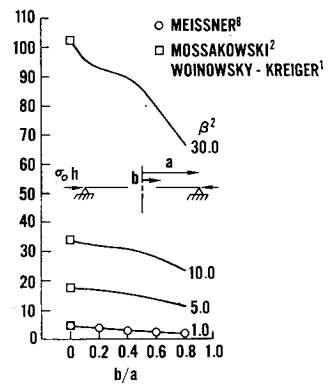

Fig. 4 Critical buckling loads, buckling parameter $\lambda = -\sigma_o h a^2/Dr$ vs b/a, outer edge simply-supported and loaded, inner edge free.

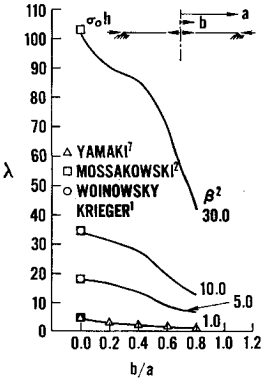

Fig. 6 Critical buckling loads, buckling parameter $\lambda = -\sigma_o h a^2/Dr$ vs b/a, outer edge simply-supported, inner edge free, both edges loaded.

‡ The computations were performed in the Computer Center of the University of Connecticut. This facility is supported in part by the National Science Foundation Grant GJ-9.

illustrates the importance of including the orthotropicity of the material in analyses.

References

[1] Woinowski-Krieger, S., "Buckling Stability of Circular Plates with Circular Cylindrical Aeolotropy," *Ingenieur-Archiv*, Vol. 26, 1958, pp. 129–131.

[2] Mossakowski, J., "Buckling of Circular Plates with Cylindrical Orthotropy," *Archiwum Mechaniki Stosowanej*, Vol. 12, 1960, pp. 583–596.

[3] Pandalai, K. A. V. and Patel, S. A., "Buckling of Orthotropic Circular Plates," *Journal of the Royal Aeronautical Society*, Vol. 69, April 1965, pp. 279–280.

[4] Uthgenannt, E. B., "Buckling and Nonlinear Behavior of Orthotropic Annular Plates," Ph.D. thesis, June 1970, University of Connecticut, Storrs, Conn.

[5] Hildebrand, F. B., *Methods of Applied Mathematics*, 2nd ed., Prentice-Hall, New Jersey, 1965, pp. 62–65.

[6] Schubert, A., "Kleine Mitterlungen," *Zeitschrift fur angewandte Mathematik und Mechanik*, Vol. 25/27, No. 4, July 1947, pp. 123–124.

[7] Yamaki, N., "Buckling of a Thin Annular Plate Under Uniform Compression," *Journal of Applied Mechanics*, Vol. 25, June 1958, pp. 267–273.

[8] Meissner, E., "Ueber das Knicken kreisring formiger Scheiben," *Schweiz Bauzeitung*, Vol. 101, No. 8, Feb. 1933, pp. 87–89.

[9] Rozsa, M., "Stability Analysis of Thin Annular Plates Compressed Along the Outer or Inner Edge by Uniformly Distributed Radial Forces," *Acta Technica Academiae Scientiarum Hungaricae*, Vol. 53, 1966, pp. 359–377.

Sphere Drag in Near-Free-Molecule Hypersonic Flow

M. I. Kussoy,* D. A. Stewart,* and C. C. Horstman†
NASA Ames Research Center, Moffett Field, Calif.

THERE are many practical applications, such as satellite drag and lifetime predictions, and density measurements in the upper atmosphere where a precise knowledge of the drag coefficient (C_D) of spheres at hypersonic Mach numbers for near-free-molecule flow conditions is required. Recent experimental investigations[1–5] have measured drag coefficients in near-free-molecular flow equal to or slightly less than the free-molecule limit (assuming diffuse reflection and an accommodation coefficient of one). These data were obtained for both hot- and cold-wall conditions at Mach numbers from 8 to 15. A few experiments at $M_\infty > 15$ by Slattery et al.,[1] and Kussoy and Horstman[6] have indicated

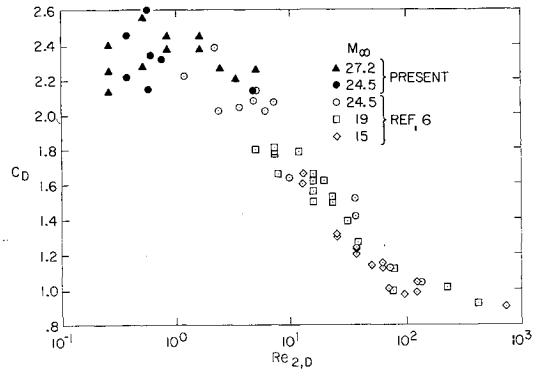

Fig. 1 Sphere-drag coefficient variation with Reynolds number.

Received June 24, 1970; revision received August 3, 1970.

* Research Scientist. Member AIAA.

† Research Scientist. Associate Eellow AIAA.

Table 1 Sphere drag-coefficient results

Condition 1: $M_\infty = 27.2$, $Re_\infty/\text{cm} = 221$, $Re_2/\text{cm} = 6.6$, $T_w/T_0 = 0.035$, $T_w/T_\infty = 5.3$, $T_w = 294°\text{K}$		Condition 2: $M_\infty = 24.5$, $Re_\infty/\text{cm} = 236$, $Re_2/\text{cm} = 9.4$, $T_w/T_0 = 0.035$, $T_w/T_\infty = 4.1$, $T_w = 294°\text{K}$	
Sphere diam., cm	C_D(meas.)	Sphere diam., cm	C_D(meas.)
0.762	2.26	0.559	2.13
0.559	2.20	0.080	2.31
0.376	2.26	0.064	2.34
0.254	2.45, 2.37	0.061	2.60, 2.14
0.130	2.45, 2.37	0.041	2.45, 2.21
0.080	2.55, 2.27		
0.040	2.40, 2.25, 2.13		

sphere drag coefficients above their free molecule limits. The purpose of this Note is to present additional data in the near-free-molecular regime for flow conditions ($M_\infty \approx 25$, $T_w/T_\infty \approx 5$) which are closer to Earth satellite conditions.

The present data were obtained using a free-flight technique in the Ames 42-in. Shock Tunnel. The operation and calibration procedures of this facility are described elsewhere.[6] The present test conditions are given in Table 1. The free-flight technique is similar to that used in Ref. 6, except for the model launch procedure which employed a retractable table similar to the one described in Ref. 7. The accuracy of the data have been calculated to be $\pm 10\%$ for the present investigation. The larger spheres (0.76–0.25 cm diam) were made from maple, pine, balsa wood, steel, zinc, copper, or plastic, and spray-painted with black paint. The smaller spheres (0.041–0.25 cm diam) were made from a synthetic sapphire-ruby material and painted with a diluted blue marking dye solution. Within experimental accuracy, no effect of surface or material on the drag could be observed.

The sphere drag results for air are presented in Table 1 and are shown on Fig. 1, plotted against $Re_{2,D}$ (the Reynolds number based on conditions behind the bow shock wave). Results obtained previously[6] are also shown. At comparable Reynolds numbers, they are in good agreement with the present results. At values of $Re_{2,D} < 1$, the drag coefficient levels off to an average value of 2.35 which is 10% above the free-molecular drag coefficient (2.12) computed for the present test conditions assuming diffuse reflection and an accommodation coefficient of one.

Hersh[2] showed that this higher drag coefficient was theoretically plausible if the energy accommodation coefficient was less than one. Free-molecule sphere drag coefficients up to 2.6 could be computed for the present test conditions assuming energy accommodation was less than one. In a similar vein, Hurlbut and Sherman,[8] using a reflection model originally proposed by Nocilla,[9] computed theoretical values of the free-molecule drag coefficient for spheres in hypersonic flow ranging from below 2.0 to about 2.8, depending on the particular reflection model chosen. It is likely that the reason for the present data being above the "free-molecule limit" while the previous data[1–5] are close to or below their "free-molecule limits," is because of the differences between the surface reflection and/or energy accommodation laws as a function of Mach number and wall temperature ratio in this flow regime. However, it is not possible to determine the particular reflection laws and coefficients from these experimental results because of the integration process involved.[2,8] Thus, for problems such as predictions of satellite lifetimes and atmospheric density measurements, the experimental sphere drag coefficients should be used whenever possible.

References

[1] Slattery, J. C., Friichtenicht, J. F., and Hamermesh, B., "Interaction of Micrometeorites with Gaseous Targets," *AIAA Journal*, Vol. 2, No. 3, March 1964, p. 543.